Studies of sea areas with airborne lidar Part 1. Short paths

G.P. Kokhanenko, I.E. Penner, and V.S. Shamanaev

Institute of Atmospheric Optics,
Siberian Branch of the Russian Academy of Sciences, Tomsk

Received September 10, 2001

Lidar returns obtained in sensing the seawaters in the region of the Hebrides Islands with an airborne lidar were processed. The series of the extinction coefficient ε measured in short time intervals above a stable sea were compared, and it was found that the field of the extinction coefficient ε in water has a cellular structure. The horizontal dimensions of the ε inhomogeneities in this experiment varied from hundreds of meters to several kilometers. The values of ε fluctuated up to 50% about the mean value. The correlation length for the extinction coefficient was about 3 km.

Introduction

In 1997 the aircraft-laboratory of the Institute of Atmospheric Optics was flown over the seas surrounding the Northern Scotland. Five flights have been performed on the total in different regions and with different tasks. One of the problems to be solved was finding how stable and repeatable can the lidar data be at multiple scattering from also stable sea area.

For this purpose, we have selected a region in the Sea of Hebrides between the Outer Hebrides and the Inner Hebrides.

In this region, the aircraft was flown for a rather short time interval (1–2 h) along the same route, but in the opposite directions. In a different variant, flights followed a ring route about a fixed center point (say, point measurements).

1. Equipment and the technique of data processing

The main research instrument was a Makrel-2 lidar operated at the wavelength of 532 nm. Various technical details on this lidar can be found, for example, in Refs. 1 and 2.

The lidar was mounted aboard an AN-30 aircraft No. 30039 of the Myachkovsky (Moscow) squadron. Trimble GPS connected to the lidar computer was used for precision positioning. As a rule, the aircraft was flown at a speed of 320 km/h (~88 m/s) at the altitude of 200–300 m above the sea level.

In this experiment, we refused to obtain depth profiles of the extinction coefficient $\varepsilon(z)$, but used the depth-mean value of the ε measured with a smaller error by a traditional algorithm of the logarithmic derivative.[3]

The airborne hydro-optical lidar sensing is complicated by a number of circumstances, in particular, by a limited dynamic range of the photomultiplier tubes in both of the polarization channels, limited range of signal recording in a 7-bit analog-to-digital converter, possibility of appearance of bright laser glints from microplates of the rough-sea oriented normally to the laser beam (this causes large absolute fluctuations in the power of underwater echoes), and, finally, forced changes in the flight altitude. Even if these changes are not very large, they lead to the changes in contribution of the multiple scattering to the echo signals.[3]

For these reasons, in numerous flights (not only those near Scotland), we have developed the following algorithm for processing the lidar echoes.

When echoes are digitized in a 7-bit ADC, a signal from 0 to 127 ADC code units (i.e., some relative power) may appear in the recording channel. The error of digitization is equal to ± 1 bit.

Let $i_1, \ldots, i_n$ be the sequence of digitization points over the depth in water and $P_1, \ldots, P_n$ be the corresponding values of the signal power; H_0 is the aircraft flight altitude; $n = 1.33$ is the refractive index of water, and $r_i = i\Delta r$ is the depth in water. In its turn, Δr is the quantization step of the analog-to-digital converter, and in this case $\Delta r = 0.8$ m. If S_i is the value of the lidar function $S(r) = P(r)(H_0 + \frac{r}{n})^2$ at the depth r_i, then the extinction coefficient ε averaged over the sensing depth can be estimated using the least-squares method as

$$\varepsilon = 0.5\,\frac{\sum_{i_1}^{i_2} r_i \sum_{i_1}^{i_2} \ln S_i - (i_2 - i_1 + 1)\sum_{i_1}^{i_2} r_i \ln S_i}{(\sum_{i_1}^{i_2} r_i)^2 - (i_2 - i_1 + 1)\sum_{i_1}^{i_2} r_i^2}.$$

For every pulse, we selected the initial point i_1 (value not constant over the depth) at the level of

0235-6880/01/12 1038-05 $02.00

about 90% of the ADC dynamic range (really $P(i_1) \le 110$ ADC code units). In the far (deepest) end of the sensing path for this laser pulse (point i_n), the signal value should naturally exceed the ADC quantization noise. We used $P(i_n) = 3$, i.e., the signal-to-noise ratio was equal to three. As a rule, the interval $i_n - i_1$ corresponded to the depth of 5 to 15 m. Its variations depended on the experimental conditions (i.e., flight altitude, water turbidity, etc.).

Besides, at the first stage, all signals were controlled to exclude the effect of PMT afterepulsing.[3]

Estimates of the error in ε measurements show that it is no larger than 12% (Ref. 3).

The obtained horizontal series of the extinction coefficient $\varepsilon(L)$, where L is the distance along the flight path, were used in two ways.

In the simplest form, they were just the horizontal profiles of the measured values of $\varepsilon(L)$, where L varied from several hundreds of meters to several hundreds of kilometers. This profiles allow estimation of the absolute value of ε, minimum and maximum dimensions of inhomogeneities for the given experiment, and averaged horizontal gradients of the extinction coefficient, i.e., its trends. They may look as both dark and light spots with $\varepsilon(L)$ values both higher and lower than the mean value, i.e., with more or less transparent water.

In a more complicated version, statistical processing of $\varepsilon(L)$ was performed, for which purpose it was first converted into the form of a random stationary process, as was done in Ref. 3. To do this, the $\varepsilon(L)$ variance was calculated for every measurement file, linear trends were subtracted from it, and the measured current values of ε were normalized to the selected variance. Thus, only the fluctuating part of the $\varepsilon(L)$ profile with the zero mean remained under consideration. Normalization of the absolute values of ε to their variance reduced the measured profiles of ε to the single dimensionless scale and allowed their comparison, joining, and further processing.

2. Results of rectilinear flights

In one of the flights over the region of the Hebrides, the aircraft passed roughly the same route several times, whose direction differed by 4° from the direction of a geographic parallel. The route traverses are shown schematically in Fig. 1*a*, along with the local (Greenwich) time for each of the traverses. The common part of the route was about 90 km long. Figure 1*b* depicts the corresponding horizontal profiles of $\varepsilon(L)$.

It is clearly seen that all these profiles tend to decrease in absolute value of the ε along the direction from west to the east (with the gradient about $1 \cdot 10^{-3}$ m^{-1}/km) and the positions of their local peaks and dips coincide. The distance between the centers of areas with the least transparent water for this figure equals 0.36–0.62 rel. degree of longitude. For the less pronounced optical inhomogeneities, the distance between them decreases down to hundreds of meters.

Using the correlation analysis, we have checked whether the values of the extinction coefficients obtained at almost the same path are statistically stable at insignificant separation between the measurement paths in both space and time. We have selected the data of measurements from parallel segments of the route traverses *3* and *4*, as the closest ones in time of sensing (less than 20 min), but most remote in space (~ 3 km, Fig. 1*a*), as well as measurements from route traverses *1* and *4*, as separated farthest apart in the time of sensing (~ 90 min), but closest in space (< 0.8 km). The length of the interval of the jointly selected values of the extinction coefficient at each segment was 10 min in time and roughly 50 km in space.

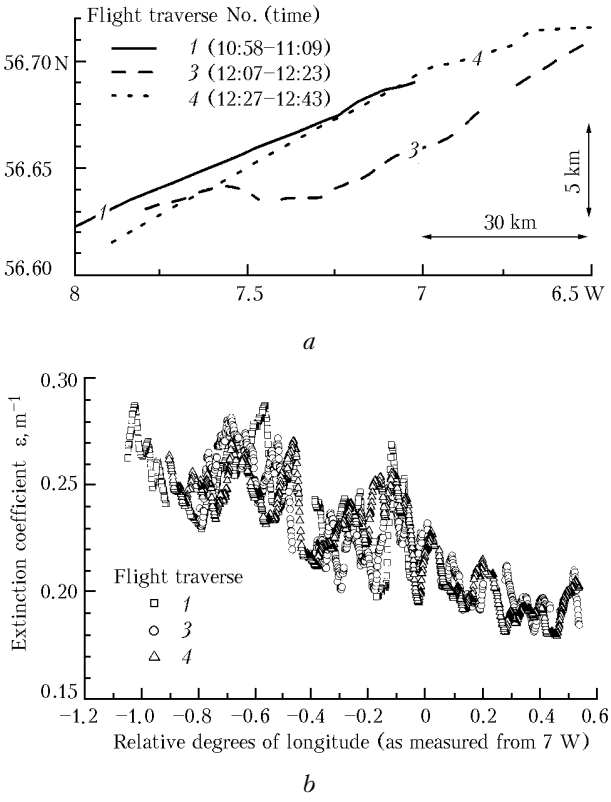

Fig. 1. Flights along the rectilinear routes: coordinate reference of the three flight traverses (*a*) and horizontal profiles of the extinction coefficient for these flight lines (*b*).

Within this interval, a continuous series of values of the extinction coefficient was formed. Preparation of the data consisted in removal of the linear trend from the series of individual realizations of ε and their centering near the zero mean. Then they were joined sequentially at the break points, if they appeared within the given space and time of measurements. Then the obtained continuous realizations at the selected pairs of route line segments were ranged along the line

according to the coordinate reference on the projection of the geographic longitude. As a result of ranging with the use of thinning and interpolation operations, the series of continuous data on fluctuations of the extinction coefficient within the equidistant arrangement of coupled points at the common flight line were obtained. Each realization prepared for the correlation analysis contained 512 points with the interval of about 100 m in space and about 1.1 s in time.

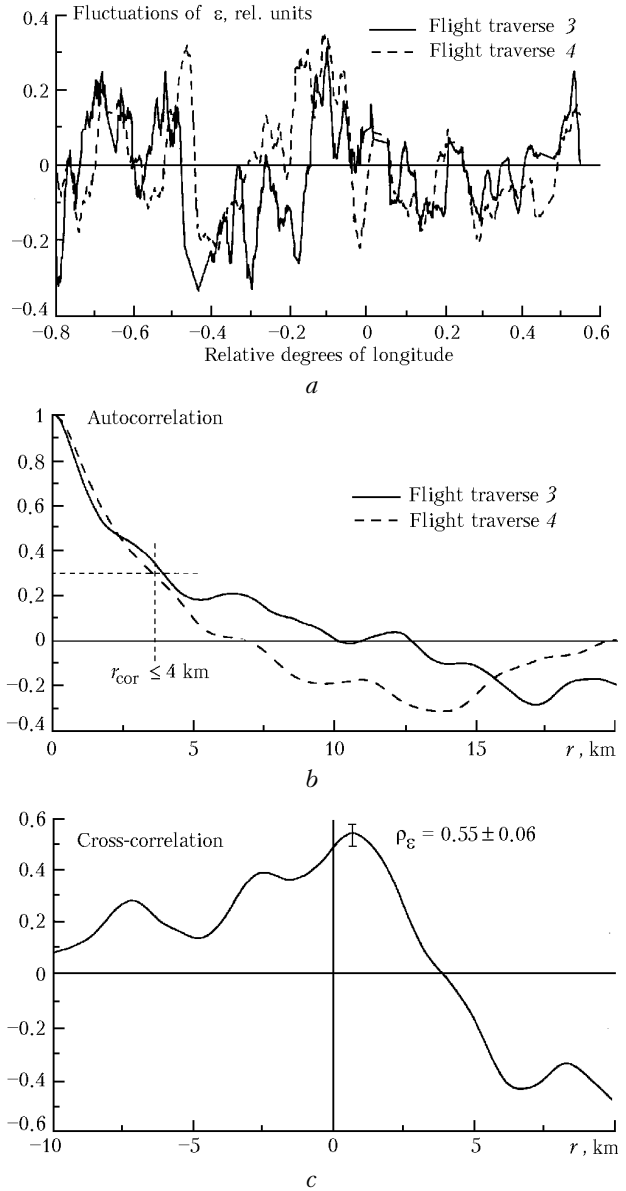

Fig. 2. Pair of flight traverses closest in time, but separated by 3 km in space: fluctuation profiles of the normalized extinction coefficient (*a*); autocorrelation functions of ε fluctuations for both of the flight traverses (*b*); cross-correlation function for values of ε in both flight traverses (*c*).

The results obtained by that sort of processing are shown in Figs. 2 and 3. From Figs. 2*a* and 3*a*, it can be seen that variations of the extinction coefficient can achieve the maximum value of 50% and have a rather complex spatial structure. This is also supported by the general view of the normalized autocorrelation functions calculated by the fast Fourier transform (FFT) method (see Figs. 2*b* and 3*b*).

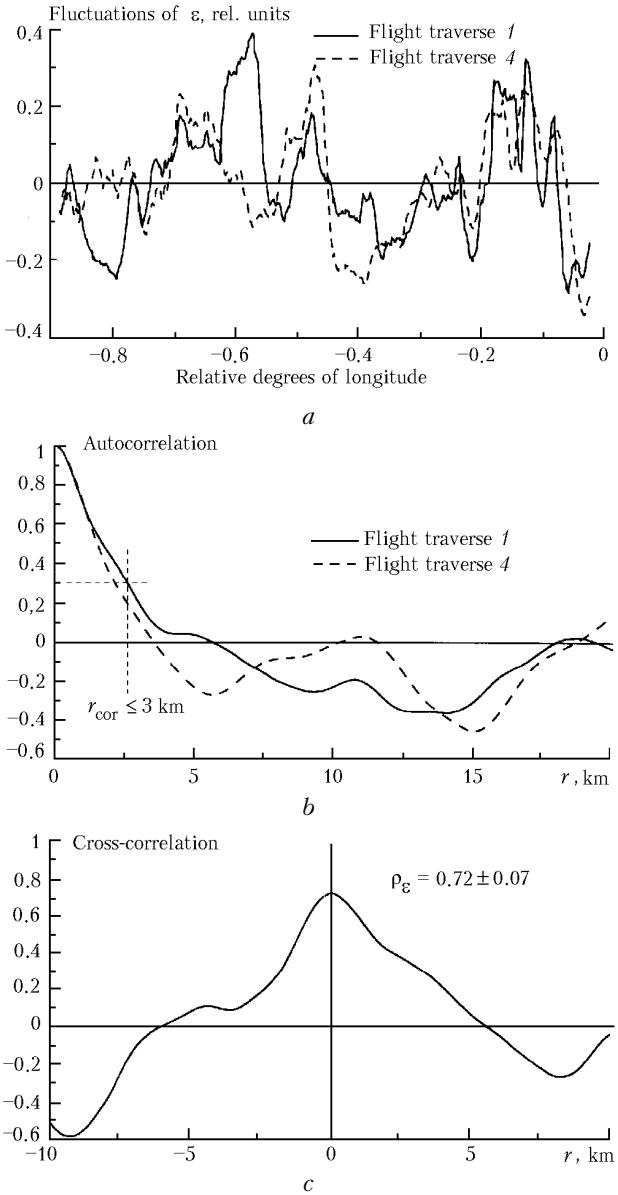

Fig. 3. Pair of flight traverses closest in space, but separated by 1.5 h in time. Designations are the same as in Fig. 2.

The periodicity in the spatial structure of the extinction coefficient is not seen clearly in the considered interval. The normalized random error of estimation of the covariation function for this realization length is about 10%. Thus, within the confidence limit of 90%, we have the correlation coefficient $\rho \geq 0.3$. The correlation length determined from the level of this statistically confident value is 3.5 km for the first pair of realizations (Fig. 2*b*) and 2.5 km for the second pair of realizations (Fig. 3*b*).

This points to the statistical dependence of measurements of the extinction coefficient within several kilometers, what agrees with the real scales of hydrological processes in the open ocean being up to 100 km.

The estimates of normalized covariation functions shown in Figs. 2*c* and 3*c* give the measure of correlation between different realizations of the extinction coefficient obtained with different space and time intervals. Thus, for two realizations measured at almost the same time (1st and 4th routes) we have high correlation and $\rho_\varepsilon = 0.72 \pm 0.07$ (Fig. 3*c*), although they were separated by 1.5 h in time. The lower correlation $\rho_\varepsilon = 0.55 \pm 0.06$ (Fig. 2*c*) is characteristic of the pair of ε realizations shown in Fig. 2*a*, in spite of the fact that they were measured within a shorter time interval (about 20 min). This can probably be explained by the fact that they were separated by far longer distance (3 km) in space. This distance between different realizations is comparable, as was revealed, with the spatial autocorrelation scale of measurements (Fig. 2*b*). Note also an insignificant shift (~ 0.6 km) of the maximum of the covariation function in Fig. 2*c*, what characterizes the presence of constant lag between different realizations separated by about 3 km in space. Unfortunately, the absence of *a priori* information on the hydrological situation at this region does not allow us to draw some conclusions on the causes of this shift and determine possible parameters of the lag. Most probably, this is the spatial inhomogeneity of the water mass in the direction normal to the aircraft flight. Nevertheless, our analysis proves, with a sufficient degree of statistical confidence, the reliability of measurements at a certain place with insignificant separation in space and more significant separation in time.

3. Results of ring flights

Several experiments were conducted to evaluate the repeatability of lidar results in other mode of sensing (when flying along a ring route). In a certain sense, these measurements can be considered as local, almost point measurements with aircraft specificity in mind.

Thus, one flight consisted of three concentric circles according to the scheme shown in Fig. 4*a* with the center at 56.96° N and 7.94°W. This point is very close to the place depicted in Fig. 1, that is, the water mass can be considered the same. In geographic coordinates, the flight lines are almost circles. In the linear coordinates, they are ellipses with the horizontal dimension of 8 km and the vertical dimension of 5.5 km (at these latitudes, one degree of latitude is already somewhat larger, in linear measure, than one degree of the longitude).

Figure 4*b* depicts the horizontal profiles of ε values obtained at the ring route. Two lower almost coinciding profiles correspond to two circles passed with the same field of view of 10.6 mrad (the telescope's field stop of 8 mm in diameter).

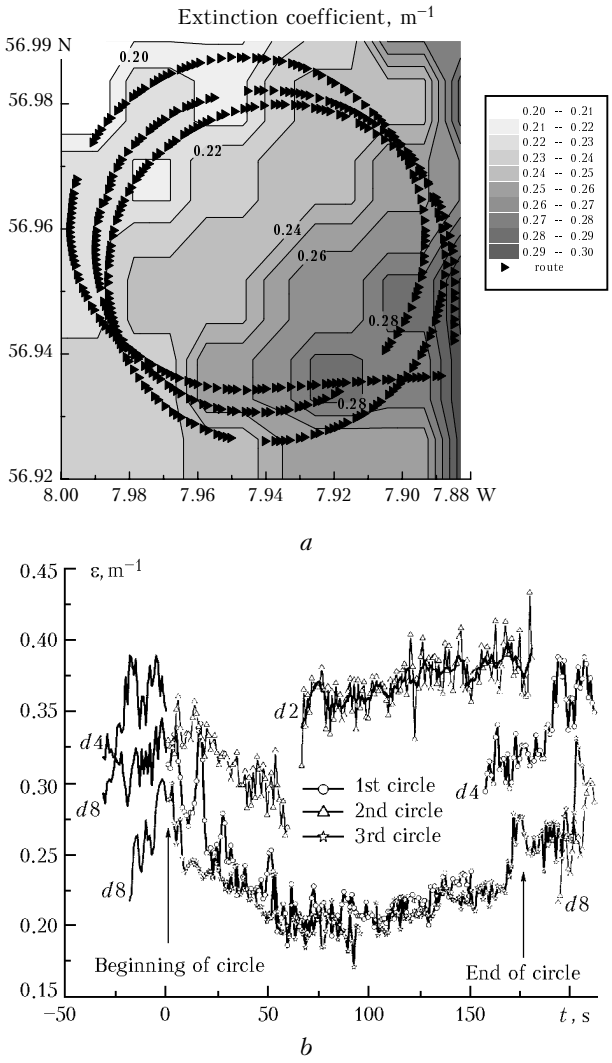

Fig. 4. Flights along concentric circles: coordinate reference of ring flight lines and reconstructed estimate of 2D distribution of the water extinction coefficient (*a*); profiles of ε along flight rings (*b*), where *d*2...*d*8 is the diameter of the field stop, in mm, that specifies the field of view of respectively 2.7, 5.3, and 10.6 mrad.

Segments with the negative time on the abscissa (to the left from the zero point) correspond to flying up to the point, from which the measurements started. They are depicted only for illustration to demonstrate the closeness of the $\varepsilon(\tau)$ profiles along the rings. Anyway, it is seen that for the two circles, whose centers are no more than 0.9 km apart, the profiles of the extinction coefficient almost coincide. We believe that in such an inert water mass, as one of local seas of the Atlantic Ocean in the littoral zone, optical properties do not change significantly for the time of about 10 min. This manifests itself in stability of our measurements of one of the basic optical characteristics – the extinction coefficient ε.

In this measurement situation, we can notice an increase in the extinction coefficient ε toward the east-southeast. This is some cell with enhanced water turbidity, in which ε increases at the distance of 6–8 km from (on the average) 0.20 m^{-1} to roughly 0.27 m^{-1}, i.e., by 35%. By the way, the presence of such cells with enhanced or lowed water transmittance was found for the first time in lidar measurements by Hoge and Swift.[4] Figure 4*a* depicts a 2D distribution of ε in this sensing area. There is only one version of this qualitative pattern, but it illustrates the water inhomogeneity in the clearest, though conditional manner.

The third ring in these measurements was devoted to studying how the field of view of the lidar's receiving telescope affects the results of sensing. The field of view here was decreased consecutively down to 5.3 and 2.7 mrad. This change of the experimental conditions had an immediate effect on the results due to the change in the effect of multiple scattering, what was explained in detail in our previous paper.[2] However, the general horizontal inhomogeneity of the sea is also seen in this area.

Earlier similar experiment was conducted in the area 30 km to the south. But in that area, water was horizontally homogeneous within the same circle of about 8 km in diameter. When the telescope's field of view was 10.6 mrad, it was found that $\varepsilon = 0.23$ m^{-1} with the standard deviation of 8.6%.

Conclusion

The experiments conducted under almost controlled conditions have demonstrated the repeatability of lidar measurements when studying the stationary water mass. The used instrumentation, technique, and algorithms allow reliable studies of the hydro-optical structure of the water mass.

References

1. A.I. Abramochkin, V.V. Zanin, I.E. Penner, A.A. Tikhomirov, and V.S. Shamanaev, Opt. Atm. **1**, No. 2, 92–96 (1988).
2. G.P. Kokhanenko, M.M. Krekova, I.E. Penner, and V.S. Shamanaev, Atmos. Oceanic Opt. **13**, No. 4, 337–346 (2000).
3. G.P. Kokhanenko, I.E. Penner, V.S. Shamanaev, G. Ladbrook, and A. Scott, Atmos. Oceanic Opt. **12**, No. 1, 37–43 (1999).
4. F.E. Hoge and R.N. Swift, Appl. Opt. **22**, No. 23, 3778–3786 (1983).